White Rose Research Online

eprints@whiterose.ac.uk
https://eprints.whiterose.ac.uk
Universities of Leeds, Sheffield and York

Deposited via The University of Leeds.

White Rose Research Online URL for this paper:
https://eprints.whiterose.ac.uk/id/eprint/79882/

Version: Accepted Version

Article:
Shi, L, Yu, Z and Jaworski, AJ (2011) Investigation into the Strouhal numbers associated with vortex shedding from parallel-plate thermoacoustic stacks in oscillatory flow conditions. European Journal of Mechanics, B/Fluids, 30 (2). 206 - 217. ISSN: 0997-7546

https://doi.org/10.1016/j.euromechflu.2010.10.005

Reuse
Items deposited in White Rose Research Online are protected by copyright, with all rights reserved unless indicated otherwise. They may be downloaded and/or printed for private study, or other acts as permitted by national copyright laws. The publisher or other rights holders may allow further reproduction and re-use of the full text version. This is indicated by the licence information on the White Rose Research Online record for the item.

Takedown
If you consider content in White Rose Research Online to be in breach of UK law, please notify us by emailing eprints@whiterose.ac.uk including the URL of the record and the reason for the withdrawal request.

UNIVERSITY OF LEEDS
University of Sheffield
UNIVERSITY of York

Investigation into the Strouhal numbers associated with vortex shedding from parallel-plate thermoacoustic stacks in oscillatory flow conditions

Lei SHI, Zhibin YU and Artur J. JAWORSKI [1]

School of Mechanical, Aerospace and Civil Engineering,

University of Manchester, Sackville Street, Manchester, M13 9PL,

United Kingdom

ABSTRACT:

This paper investigates vortex shedding processes occurring at the end of a stack of parallel plates, due to an oscillating flow induced by an acoustic standing wave. Here the hot-wire anemometry measurement technique is applied to detect the velocity fluctuations due to vortex shedding near the end of the stack. The hot-wire fast time response enables obtaining detailed frequency spectra of the velocity signal, which can be used for identifying the dominant frequencies associated with vortex shedding, and thus allow calculating the corresponding Strouhal numbers. By varying the stack configuration (the plate thickness and spacing) and the acoustic excitation level (the so-called drive ratio), the impact of the stack blockage ratio and the Reynolds number on the Strouhal number has been studied in detail. Furthermore, in the range of the Reynolds numbers between 200 and 5,000 a correlation between the Strouhal number and Reynolds number has been obtained and compared with analogous relationships in the steady flow. Particle Image Velocimetry (PIV) is also used to visualize the vortex shedding processes within an acoustic cycle, phase-by-phase, in particular during the part of the cycle when the fluid flows out of the stack – selected cases are shown for comparisons with hot-wire measurements.

Keywords: Oscillatory Flow; Parallel-Plate Stack; Vortex Shedding; Strouhal Number; Thermoacoustic Stacks

1. Introduction

Vortex shedding from bluff bodies, and the associated vortex shedding frequency, have been a subject of many investigations since the pioneering work carried out by Vincenc Strouhal and published in 1878 [1]. This investigated the relation between the tone of a "singing" wire and fluid flow velocity – the sound produced by the wire being directly

[1] Corresponding author: a.jaworski@manchester.ac.uk; Tel:+44(0)161 275 4352; Fax:+44(0)161 306 3755

Advanced Manuscript

related to the vortex shedding frequency. The non-dimensional analysis led to what today is described as Strouhal number:

$$\mathrm{St} = fd / U_0 . \quad (1)$$

where f, d and U_o are shedding frequency, characteristic dimension (e.g. cylinder diameter) and free stream velocity, respectively. Rayleigh [2] pointed out that the Strouhal number should be a function of the Reynolds number. The earliest fluid dynamical studies of the vortex shedding processes from circular cylinders are usually attributed to von Karman (cf. Kovasznay [3]) who observed the characteristic flow patterns referred to as "von Karman vortex street".

Kovasznay [3] carried out some of the earliest quantitative investigations of the regular vortex street pattern behind a circular cylinder using hot-wire technique. His studies of Strouhal number covered Reynolds numbers up to 10^4. He obtained the critical Reynolds number of 40 at which vortices are shed, and the correlation between the Strouhal number, and Reynolds number from the critical value of 40 to around 10,000. Roshko [4] used standard hot-wire techniques to study the wake development behind the circular cylinder at low Reynolds number in a low-speed wind tunnel. Two distinct Reynolds number ranges according to different periodic wake phenomena behind circular cylinders were observed. The first one is the stable Reynolds number range from 40 to 150, in which the classical stable von Karman vortex street is formed and no turbulence develops. In the second range (above Reynolds number of around 300) the periodic shedding is accompanied by irregular or turbulent velocity fluctuations. The correlations between the Strouhal number and Reynolds number in two Reynolds number ranges were given. Roshko also pointed out that the effect of other geometrical parameters, such as the blockage ratio, on the Strouhal number must be taken into account.

Williamson [5] carried out a study on the transition range between the "stable" and "irregular" regions and confirmed that there exists a complex relationship between the Strouhal number and Reynolds number in the range from 150 to around 300. West and Apelt [6] investigated the effects of tunnel blockage on the mean flow past a circular cylinder. In a range of blockage from 2 to 16%, its effect on the pressure distribution, drag coefficient and Strouhal number was revealed. Okajima [7] conducted the experiments on the vortex-shedding frequencies and corresponding Strouhal numbers of various rectangular cylinders in a wind tunnel and in a water tank. The hot-wire anemometer was used for measuring shedding frequencies, and its signal and the corresponding frequency spectra were analyzed. Relationships between Strouhal and Reynolds numbers for different rectangular cylinders were obtained. Al-Asmi and Castro [8] investigated the flow past bluff bodies of different geometries including flat plate, tee-shaped body, as well as triangular and rectangular cross-sections. The variations of Strouhal number with Reynolds number and wind tunnel blockage was obtained. In a relatively recent research, Ferreira and Vieira [9] investigated the flow around modified circular cylinder

Advanced Manuscript

having a longitudinal notch using hot-film anemometry. The relationship between Strouhal and Reynolds numbers up to Reynolds number of 1, 000 was obtained.

In oscillatory flows Strouhal number can have two meanings, which is often a source of confusion in the literature. Firstly, it may be used to define the underlying flow forcing: $St_{excit} = f_{excit} D/U$, where f_{excit} is the underlying frequency of the oscillatory motion (flow excitation), D is the characteristic dimension (for example cylinder diameter or channel width) and U is a characteristic velocity, typically the amplitude of the velocity oscillation. It is also common to replace Strouhal number by Keulegan-Carpenter number (KC) which in effect represents an inverse of St_{excit}. Secondly, Strouhal number may actually refer to vortex shedding processes occurring during part of the oscillation cycle on the bluff body under investigation. In this second meaning the frequency used in Strouhal number definition is the actual vortex shedding frequency as envisaged in the original definition (1), although some additional discussion is needed regarding the selection of representative frequency values and reference velocities. It is the latter of the two definitions of the Strouhal number that is considered in this paper.

Studies of Strouhal number in oscillatory flows are relatively limited, for which there are perhaps two main reasons: Firstly, oscillatory flows past bluff bodies typically lead to much more complex vortex shedding phenomena than in steady flows and therefore their phenomenological description is not as straightforward as the classical von Karman vortex street. For example, Williamson and Roshko [10] observed the vortex formation in the wake of an oscillating cylinder in stationary fluid. Various vortex patterns behind the oscillating cylinder were found, such as the formation of a single vortex, vortex pairs or combination of single vortices and vortex pairs and so on. Similar studies were conducted by Okajima et al. [11] who investigated the morphology of vortex patterns for circular and square cylinders in an oscillatory flow using flow visualizations and linked their appearance with the unsteady structural loading. Chung and Kang [12] and Barbi et al. [13] carried out studies of the vortex shedding and its interesting "lock-on" effects behind a cylinder in the oscillatory incoming flow using a numerical analysis.

The second difficulty related to defining Strouhal numbers for oscillatory flows is their transient nature: considering one side of the bluff-body, vortex shedding occurs only during part of the cycle, while the underlying shedding frequency may change with time as the instantaneous free stream velocity changes. Thus there is a degree of subjectivity in choosing the method of calculating the shedding frequency from experimental data and choosing the reference velocity for the subsequent Strouhal number calculations. Some examples will be given below in the context of thermoacoustics research.

Advanced Manuscript

Similar complex vortex shedding phenomena in the oscillatory flow also appear in thermoacoustic systems where an oscillatory flow induced by the high-amplitude acoustic excitation interacts with internal structures, such as stacks, regenerators and heat exchangers. These internal structures (generally referred to as a "thermoacoustic core") allow a "thermoacoustic effect" to take place [14, 15], in which appropriately phased pressure and velocity oscillations enable the compressible fluid to undergo a thermodynamic cycle within the interstices of such internal structures. The simplest geometries of such structures are parallel plates and hence oscillatory flows around "parallel plate stacks" are of great interest within thermoacoustics. Unfortunately, fluid flow processes in the thermoacoustic stacks are not fully understood due to their complexity induced by the geometrical discontinuities (end of stack) combined with the oscillatory nature of the flow.

Previous investigations focused mainly on the application of "full field of view" techniques such as Particle Image Velocimetry (PIV) around parallel plate stacks. For example, Blanc-Benon et al. [16] investigated the flow structures shed from a stack of parallel plates, while Berson and Blanc-Benon [17] studied "non-periodicity" of the flow within the gap of a thermoacoustic couple. Interestingly, the latter work tried to derive vortex shedding Strouhal number: the frequency was estimated by "counting" the vortex structures on PIV images taken at two different phases of the acoustic cycle, while the reference velocity was taken as the convection velocity of the vortices. Unfortunately such a methodology leads to rather unrealistic St numbers (compared to classic von Karman shedding) around 0.4. Studies of Mao et al. [18] demonstrated the processes of vortex evolution during the part of the acoustic cycle where vortices are shed from stack plates, using two stacks with 1 and 5 mm thick plates, and with fixed spacing between the plates (5 and 10 mm, respectively). They observed two different evolutions of vortex patterns for 1 and 5 mm plate, respectively. Results of Aben et al. [19] showed four categories of the vorticity plots at the stack end: "two vortices", "four vortices", "transition area" and a "vortex street". Shi et al. [20] carried out systematic investigations of vortex wake patterns and their transitions occurring at the end of the parallel-plate thermoacoustic stacks, giving a total of 108 experimental conditions. They revealed the significant effects of some non-dimensional parameters, such as the Reynolds number and Womersley number (the ratio of the spacing between adjacent plates to the viscous penetration depth), on vortex wake patterns and their transitions. Vortex phenomena near the end of a thermoacoustic stack were also a subject of numerical simulations [21, 22]. Worlikar et al. [21] used a low Mach-number compressible flow model to investigate the effects of the acoustic amplitude, the stack blockage ratio, stack position in the resonator and boundary layer thickness on the unsteady flow around the thermoacoustic stack. Besnoin and Knio [22] carried out unsteady simulations of the flow field in the neighborhood of the stack and heat exchangers. They found the appearance of a large-amplitude wavy motion within the gap, between the plates and in the vicinity of the thermoacoustic stack, and the occurrence of cycle-to-cycle variability at the relatively high acoustic amplitude.

Advanced Manuscript

However, it should be noted that vortex shedding processes could be investigated using much simpler hot-wire anemometry techniques, which could provide high temporal resolution in order to investigate the spectra of velocity fluctuations behind the stack and subsequently obtain the corresponding Strouhal number values. Standard PIV techniques are usually too slow to provide time-resolved signals in thermoacoustic applications where excitation frequencies are often of the order of tens of Hertz. Surprisingly, there is only very limited number of hot-wire studies of vortex shedding from stack plates. Mao et al. [18] provided a very fragmentary set of hot-wire data for selected flow conditions around the two stack configurations discussed above. The relation between the Strouhal number (based on velocity amplitude near the end of the channel between plates) and the Reynolds number (based on the plate thickness) is plotted revealing two distinct levels of St: around 0.1 and 0.2 for two plate thickness values investigated. The key question that remained unanswered was whether there is a discrete change in St, due to some sort of "threshold" value of the plate thickness, or is there a "smooth transition" in the range of St, when the plate thickness is varied in small steps? In this sense, present paper is a further development of earlier work [18]: it investigates a wider parameter range (the plate thickness: 0.5, 1, 2, 3, 4 and 5 mm, and plate spacing between 1.2 and 10.8 mm) and tries to cover more systematically the Reynolds number range up to 5,000. It also attempts to obtain an experimental correlation between St and Re numbers. In addition, the effect of the channel blockage ratio on the Strouhal number at a given Reynolds number is studied.

2. Experimental apparatus and measurement procedure

The experimental rig is shown schematically in Fig. 1. The 7.4 meters long resonator is a metal tube with a square internal cross section of 134mm x 134mm. It is joined with a cube-shaped loudspeaker box, on which an 18 inch diameter, 600 W loudspeaker (Model PD1850) is mounted to generate an acoustic standing wave within the resonator. The acoustic coupling between the resonator and the loudspeaker generates a quarter-wavelength acoustic wave with the fundamental frequency 13.1 Hz. The resonator is filled with air at atmospheric pressure and at room temperature. The resonator is equipped with a piezoresistive pressure transducer (Endevco Model 8510B-2) to measure the pressure amplitude at one end of the resonator, which is used as a reference signal to trigger PIV measurements, phase locked to the acoustic cycle. The stack is placed in the resonator 4.6 meters (about 0.17 of the wavelength) from the end cap of the resonator.

Figure 2 shows schematically the configuration and the key geometrical parameters of the stacks. The stack plates are cut out of metal sheets, machined to ensure uniform sizes and square edges. The length of each plate (l) is 200 mm, while their width is 132 mm; six different plate thicknesses (d) were used: ≈ 0.5, 1, 2, 3, 4 and 5 mm (exact thickness values shown in Table 1). Each plate has four holes drilled for mounting "pillars" which support the whole stack structure. The distance between adjacent plates (D) is maintained by "spacers" made out of cut-outs of a 1.2 mm thick

Advanced Manuscript

perforated sheet (this ensured a uniform thickness of the spacers). The plate spacing was therefore a multiple of 1.2 mm. Overall – nine different plate spacings were tested: from 1.2 to 10.8 mm. Table 1 summarizes the stack geometries and flow conditions used in this work.

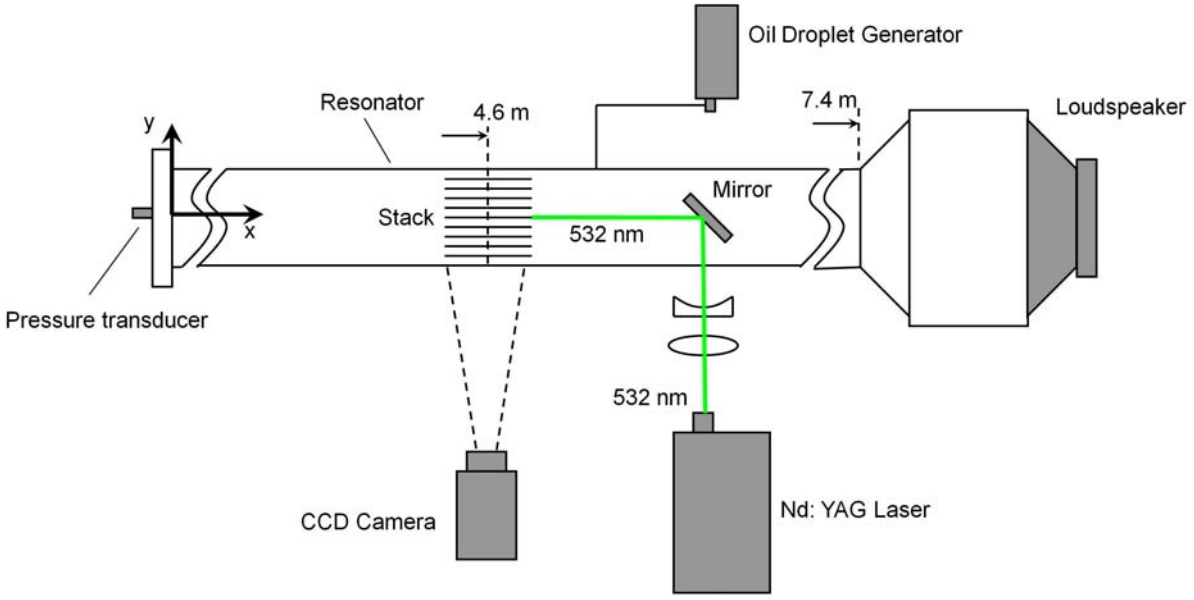

Figure 1 Sketch of the experimental apparatus

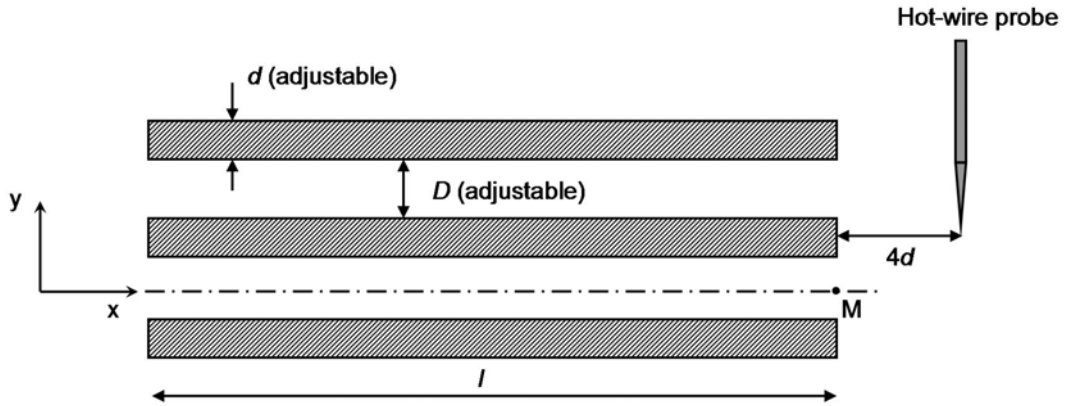

Figure 2 Geometry of the stack (only three plates shown)

In Table 1, the drive ratio (Dr), is defined as the ratio of the peak pressure amplitude to the mean pressure, which is usually used to characterize the intensity of the acoustic standing wave in thermoacoustic systems. The blockage is defined as the cross sectional area of the stack occupied by the plates over the cross-sectional area of the resonator. For parallel plate stacks it can be written as $d/(d+D)$. For a given stack geometry the flow velocity amplitude and the corresponding Reynolds number can be controlled by varying the drive ratio. The Reynolds number, Re, is defined as

$$\mathrm{Re} = u_{aM} d / \nu \,, \tag{2}$$

where ν is the kinematic viscosity of air at ambient conditions, u_{aM} is the velocity amplitude (i.e. peak value of velocity) at point M in Fig. 2 (measured using PIV as described below). Essentially, equation (2) represents the peak Reynolds number of the oscillatory flow. Ratio δ_v/D in Table 1 is the ratio of Stokes layer thickness to plate spacing.

Table 1 Summary of stack dimensions and experimental conditions; symbol "#" is used to identify the "case number" for the subsequent discussion of results.

#	d (mm)	D (mm)	$d/(d+D)$	δ_v/D	Dr (%)	u_{aM} (m/s)	Re
1	0.51	1.2	0.3	0.51	1.5	6.14	207
2	0.51	1.2	0.3	0.51	2	8.37	281
3	0.51	2.4	0.18	0.25	2	7.32	246
4	0.51	2.4	0.18	0.25	3	10.61	357
5	0.51	3.6	0.12	0.17	2	5.76	194
6	0.51	3.6	0.12	0.17	3	8.71	293
7	0.51	3.6	0.12	0.17	3.5	10.19	343
8	0.51	4.8	0.1	0.13	3	9.39	316
9	0.99	1.2	0.45	0.51	1	5.03	328
10	0.99	1.2	0.45	0.51	2	7.77	507
11	0.99	2.4	0.29	0.25	1	4.31	281
12	0.99	2.4	0.29	0.25	1.5	6.23	407
13	0.99	2.4	0.29	0.25	2	8.53	557
14	0.99	2.4	0.29	0.25	3	12.28	801
15	0.99	3.6	0.22	0.17	1	3.1	203
16	0.99	3.6	0.22	0.17	1.5	4.88	318
17	0.99	3.6	0.22	0.17	2	6.1	398
18	0.99	3.6	0.22	0.17	2.5	8.13	531
19	0.99	3.6	0.22	0.17	3	9.32	608
20	0.99	3.6	0.22	0.17	3.5	11.38	743
21	0.99	3.6	0.22	0.17	4	13.01	849
22	0.99	4.8	0.17	0.13	1.5	4.95	323
23	0.99	4.8	0.17	0.13	2	6.63	433
24	0.99	4.8	0.17	0.13	3	10.39	678
25	0.99	7.2	0.12	0.08	2	5.92	386
26	0.99	7.2	0.12	0.08	3	9.42	615
27	2.21	2.4	0.48	0.25	0.6	3.07	447
28	2.21	2.4	0.48	0.25	1	4.82	702
29	2.21	2.4	0.48	0.25	1.5	7.23	1053
30	2.21	2.4	0.48	0.25	2	8.89	1295
31	2.21	4.8	0.32	0.13	1	3.77	550
32	2.21	4.8	0.32	0.13	1.5	5.72	833
33	2.21	4.8	0.32	0.13	1.8	6.93	1010
34	2.21	4.8	0.32	0.13	2	7.78	1133
35	2.21	4.8	0.32	0.13	2.2	8.65	1260
36	2.21	4.8	0.32	0.13	2.5	9.93	1447
37	2.21	4.8	0.32	0.13	2.8	11.24	1638
38	2.21	4.8	0.32	0.13	3	12.18	1774
39	2.21	4.8	0.32	0.13	3.2	13.13	1913
40	2.21	4.8	0.32	0.13	3.5	14.52	2116
41	2.21	6	0.27	0.10	1.5	5.35	780
42	2.21	6	0.27	0.10	2	7.41	1079
43	2.21	6	0.27	0.10	3	11.43	1666
44	2.21	8.4	0.21	0.07	1.5	4.85	707
45	2.21	8.4	0.21	0.07	2	6.62	965
46	2.21	8.4	0.21	0.07	3	10.39	1513

Advanced Manuscript

47	3	4.8	0.38	0.13	1	4.1	810
48	3	4.8	0.38	0.13	2	8.54	1690
49	3	4.8	0.38	0.13	3	12.24	2420
50	3	4.8	0.38	0.13	4	16.32	3227
51	3	6	0.33	0.10	3	12.76	2523
52	3	8.4	0.26	0.07	1.5	5.19	1026
53	3	8.4	0.26	0.07	2	7.15	1414
54	3	8.4	0.26	0.07	3	10.96	2167
55	4.06	4.8	0.46	0.13	1.5	6.95	1859
56	4.06	4.8	0.46	0.13	2	9.4	2514
57	4.06	6	0.4	0.10	1.8	7.62	2040
58	4.06	6	0.4	0.10	2	8.47	2267
59	4.06	6	0.4	0.10	2.2	9.32	2494
60	4.06	6	0.4	0.10	2.4	10.17	2721
61	4.06	6	0.4	0.10	2.6	11.01	2947
62	4.06	6	0.4	0.10	2.8	11.86	3174
63	4.06	6	0.4	0.10	3	13.35	3573
64	4.06	6	0.4	0.10	3.2	13.96	3736
65	4.06	6	0.4	0.10	3.5	14.82	3968
66	4.06	7.2	0.36	0.08	1	4.09	1095
67	4.06	7.2	0.36	0.08	1.5	6.24	1671
68	4.06	7.2	0.36	0.08	2	8.49	2273
69	4.06	7.2	0.36	0.08	3	12.79	3424
70	4.06	9.6	0.3	0.06	1.5	5.21	1395
71	4.06	9.6	0.3	0.06	2	7.11	1904
72	4.06	9.6	0.3	0.06	3	11.08	2966
73	5.12	10	0.34	0.06	2	6.2	2228
74	5.12	10	0.34	0.06	3	9.54	3341
75	5.12	10.8	0.32	0.06	2	13.36	4509
76	5.12	10.8	0.32	0.06	3	12.09	4081

To investigate the vortex shedding frequencies, a standard hot-wire anemometry system by TSI, IFA300, was used to detect fluid velocity fluctuations near the end of the stacks. The sensor was Dantec 55P11 probe with 5 μm diameter tungsten wire. The hot-wire probe is placed normal to the plate and the axis of the resonator. Its distance from the edge of the plate was 4*d*, as shown in Fig. 2. This distance has been chosen after preliminary measurements to establish the region where the highest velocity fluctuation levels exist for various plate thickness values – 4*d* came out as one of the most representative locations. The signals from the hot-wire anemometer were recorded with a sampling frequency of 5,000 Hz by a data acquisition card (Omega DAQTemp14A). 16,384 data points were acquired for each experimental run. Finally, hot-wire signals were analyzed using with Fast Fourier Transform (FFT) method in order to extract peak frequency in the frequency-spectrum.

Advanced Manuscript

In order to visualize the vortex shedding processes corresponding to hot-wire signal traces, flow field measurements were performed using PIV system by LaVision. As shown in Fig. 1, the laser sheet is generated by a dual Nd:YAG laser with a wavelength of 532nm, and combined with sheet optics and divergence lens. It enters the resonator perpendicularly to its axis, is reflected by a small mirror and becomes parallel to the resonator axis and normal to the surface of the stack plates. Images are taken by LaVision Imager Pro plus camera with a 4 mega-pixel CCD sensor and post processed using commercial software LaVision DaVis 7.2. The flow is seeded with olive oil droplets, produced by an oil droplet generator (TSI's model 9307). The mean droplet diameter is 1 micron. Cross-correlation mode is used and the interrogation window is 16 pixels by 16 pixels. The field of view of the PIV images varied from 15mm× 15mm to 60mm× 60mm, depending on the flow features to be imaged. The maximum spatial resolution was 0.12 mm.

PIV flow field measurements were performed at 20 phases in one acoustic cycle as illustrated in Fig. 3. For each phase, 100 pairs of frames were taken to calculate the phase-averaged velocity vector fields. For the convenience of explaining the hot-wire signal traces and corresponding flow patterns by PIV, two flow stages are defined according to fluid flow direction. In Fig. 2, when the velocity at point M is toward the positive direction of x coordinate (corresponding to phases Φ_1 through to Φ_{10} as illustrated in Fig. 3), it is referred to as an "ejection" stage; whereas when it is toward the negative direction of x coordinate (corresponding to phases Φ_{11} through to Φ_{20}), it is referred to as a "suction" stage. For convenience of further explanation, the ejection stage can be further subdivided into acceleration stage (phases Φ_1-Φ_5) and deceleration stage (phases Φ_6-Φ_{10}).

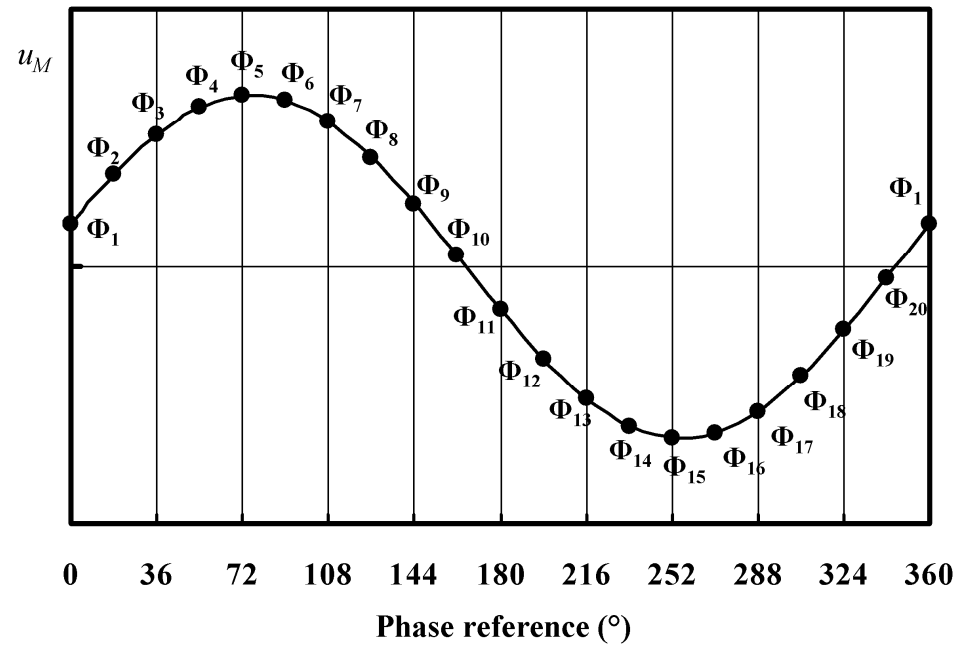

Figure 3 Phase-averaged velocity at point M and 20 tested phases (d=1mm, D=4.8mm, Dr=0.6%).

Advanced Manuscript

3. Experimental results and discussion

As shown in Table 1, 76 experimental cases were studied in total. To avoid introducing a large number of figures, the presentation of experimental results starts with a detailed analysis of one typical flow case, which includes the shedding frequency measurement, data processing procedure, and corresponding PIV visualization of the vortex shedding process phase by phase. This typical case, shown in section 3.1, illustrates the detailed procedures undertaken to process the experimental data for each of the 76 cases. Following this, section 3.2 discusses the relationship between Strouhal and Reynolds numbers for several different stacks. In section 3.3, the impact of the blockage of the stack on the relationship between Strouhal and Reynolds number is discussed. Finally, section 3.4 analyses a complete map of Strouhal number versus Reynolds number dependence for all of the tested cases. Here the Strouhal number in Equation (1) is based on the plate thickness, d, the velocity amplitude at the entrance to the stack, u_{aM}, and vortex shedding frequency, f, which is obtained from frequency spectra of the hot wire signal.

3.1 Detailed analysis of a typical case

The experimental case discussed in detail in this subsection is the case 23, which is the stack with d=1mm, D=4.8mm at the acoustic excitation level Dr=2.0% and the resulting peak Reynolds number Re=433. Figure 4a shows the original hot-wire signal trace in one acoustic cycle. Due to the nature of a single hot-wire measurement, which does not detect the flow direction, signals at both the "ejection" and "suction" stages have the same positive sign, somewhat similar to the absolute value of a sinusoidal wave. It can be seen that there is a strong "fluctuation burst" in the first half of the cycle ("ejection" stage), when the fluid flows out of the stack and the vortices are shed from the plates. It is also found that the relatively large fluctuations of hot-wire signal do not appear until Φ_4, but subsequently dominate the signal in the whole of the decelerating stage (90°-180°). For the second half of the acoustic cycle ("suction" stage), there is some small fluctuation in the acceleration phase (180°-270°), while the signal trace is quite smooth in the deceleration phase (270°-360°).

As mentioned above, PIV measurement has also been carried out to gain an insight into the corresponding vortex shedding processes. For the convenience of this comparison, six phases (Φ_2, Φ_4, Φ_5, Φ_7, Φ_8 and Φ_{10}) in the "ejection" stage and four phases (Φ_{11}, Φ_{13}, Φ_{16} and Φ_{19}) in the "suction" stage are marked by the dashed lines in Figure 4 (a). The PIV pictures corresponding to these phases are shown in Figure 5, discussed later.

Advanced Manuscript

Judging from Fig. 4a, the obtained hot wire signal combines the effects of acoustic velocity (at 13.1 Hz) and the velocity fluctuations due to vortex shedding. Therefore, to aid analysis, before applying the fast Fourier transform (FFT) algorithm to extract vortex shedding frequency, the oscillatory sinusoidal signal with the fundamental frequency 13.1 Hz is removed. This could in principle be done in two ways: by applying a high pass signal filter before the data acquisition, or by using a digital high pass filter during data post-processing. During this work a high pass filter was applied to the signal within the data acquisition loop, with the set threshold frequency of 15 Hz. The filtered hot wire signal (with the acoustic velocity component removed) is shown in Fig 4b: the high frequency fluctuations are clearly visible.

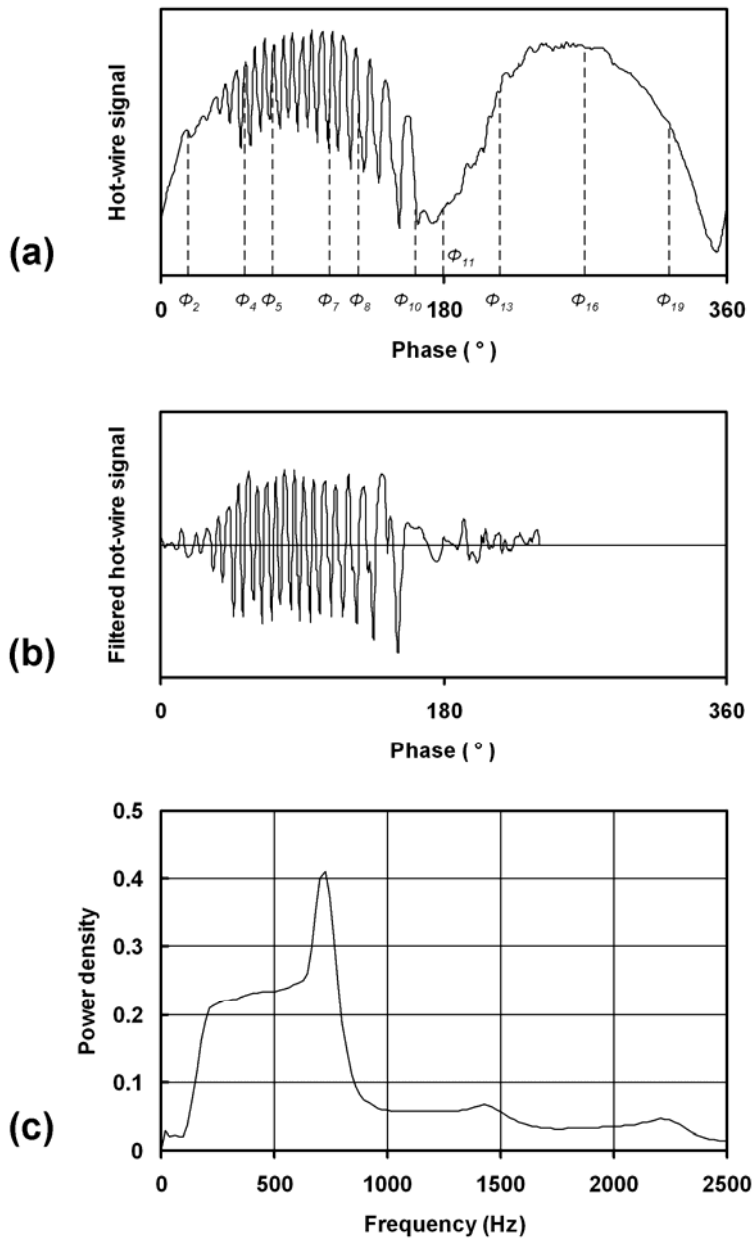

Figure 4 Hot-wire signal within an acoustic cycle and the corresponding frequency spectrum (*d*=1mm, *D*= 4.8mm, Dr=2.0%, Re=433); a – original hot-wire signal; b – filtered hot-wire signal; c – frequency spectrum

It is worth adding that Figs. 4a and 4b only show a sample from one acoustic cycle. However, for each experimental run 100 cycles have been recorded. To ensure that the FFT is applied to a statistically meaningful set of fluctuations, the 100 cycles of filtered signal traces have been divided into data blocks. Each data block has 256 data points, which starts from the same phase in each acoustic cycle, and covers the whole "fluctuation burst" (such as shown in Figure 4b). For each data block, a frequency spectrum can be obtained after the application of FFT. For each run, 100 frequency spectra can be obtained. To cancel the effects of cycle-to-cycle variability, the 100 frequency spectra obtained are averaged, giving a mean frequency spectrum such as shown in Fig. 4c.

Figure 5 gives the vorticity fields for the same case as shown in Fig. 4 for the phases highlighted in Fig. 4a. At the beginning of the ejection stage (Fig. 5a – Φ_2), the flow starts to accelerate and forms a pair of attached vortex structures at the end of the plate. They are symmetrical relative to the centre-line of the plate. This corresponds to a relatively smooth rise in the hot-wire signal trace in Fig. 4a. As the velocity gradually increases the flow pattern changes accordingly. The attached symmetrical vortex structures (Fig. 5b – Φ_4) start to break up into discrete vortices, which look as though they were shed alternately from the top and the bottom side of each plate. It corresponds to occurrence of fluctuations in hot-wire signal traces in Fig. 4a (Φ_4). As the flow velocity increases further in Fig. 5c (Φ_5), the vortex shedding pattern extends relatively far from the plate, in a similar fashion to the classical "vortex street". This corresponds to a high amplitude of hot-wire signal fluctuations as can be seen in Fig. 4a (Φ_5). When the flow enters the deceleration stage, the velocity starts to decrease. However vortex shedding still remains a dominant feature with vortex structures extending further from the plates as illustrated in Figs. 5d and 5e (Φ_7 and Φ_8). This agrees well with the hot wire signal in Fig. 4a, where the strong fluctuations dominate in the whole deceleration stage. At the end of the deceleration stage – see Fig. 5f (Φ_{10}) – the flow slows down and the "vortex street" gradually disappears. After this phase, the flow reverses and starts to enter the "suction" stage of the cycle, as seen in Fig. 5g (Φ_{11}). The hot-wire signal trace gives nearly a minimum value at this phase. When the fluid velocity increases (in the direction towards the stack) a pair of attached counter-rotating vortex structures at the end of the plate are formed (see Fig. 5h – Φ_{13}), which corresponds to smooth changes of hot-wire signal traces in Fig. 4a (Φ_{13}). Further increase and subsequent decrease of the fluid velocity does not affect the flow structure significantly as shown in Figs. 5i and 5j (Φ_{16} and Φ_{19}, respectively). The hot-wire signal is relatively smooth, until the flow enters the next acoustic cycle.

Advanced Manuscript

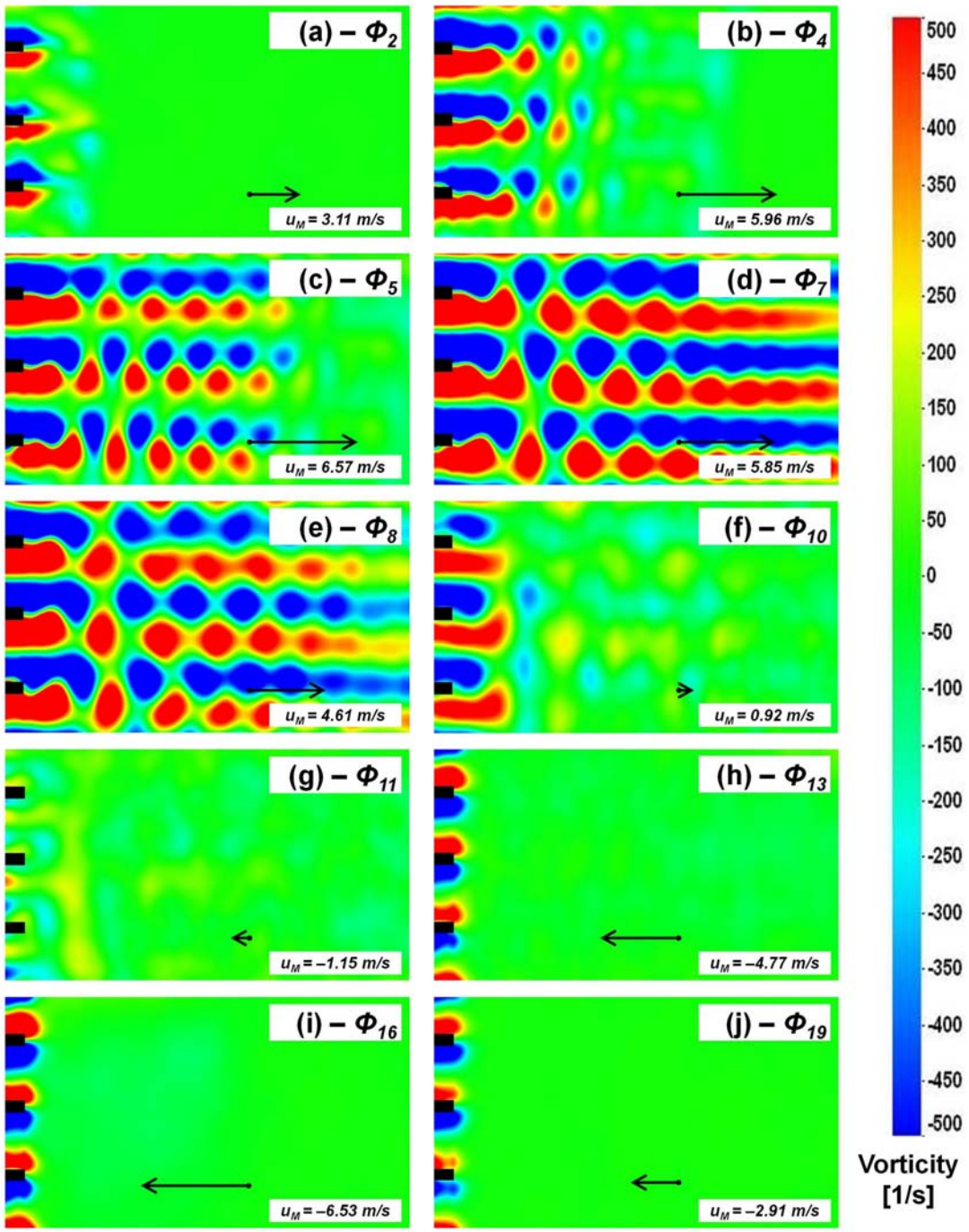

Figure 5 Vorticity fields for the flow at the end of the stack; *d*=1mm, *D*=4.8mm, Dr=2.0%, Re=433, the particle displacement amplitude equals to 81 mm; Arrows in the frames indicate the magnitude and direction of phase-averaged velocity u_M corresponding to this frame; values of u_M are given next to the arrows.

3.2 The relationship between Re and St for a given configuration of stack

In this subsection, the relationship between Reynolds number and Strouhal number is shown for three different sizes of stacks, which are referred to as stack A (d = 1mm, D = 3.6 mm), stack B (d = 2mm, D = 4.8mm) and stack C (d = 4mm, D = 6mm).

Figure 6 shows hot-wire signal traces within an acoustic cycle and the corresponding frequency spectra obtained for stack B for three different Reynolds numbers, which correspond to flow cases 31, 34 and 38 in Table 1. Clearly, the fluctuation frequencies of the hot-wire signal traces increase with the increase of Re, which can be seen both in the time-domain (Figs 6a, c and e) and the frequency domain (peak frequencies visible in spectra in Figs. 6b, d and f). However, it is also interesting to note that the frequency spectra for each of the three Re values exhibit some form of "broad-band" character (in particular Fig. 6f). This is different from sharp peaks which would normally be obtained in the steady flows past bluff bodies. This wide band of frequencies could be due to variations in the shedding frequency as an instantaneous velocity changes in the ejection stage, although it could also be an effect of averaging the instantaneous flow field characteristics that may change from cycle to cycle.

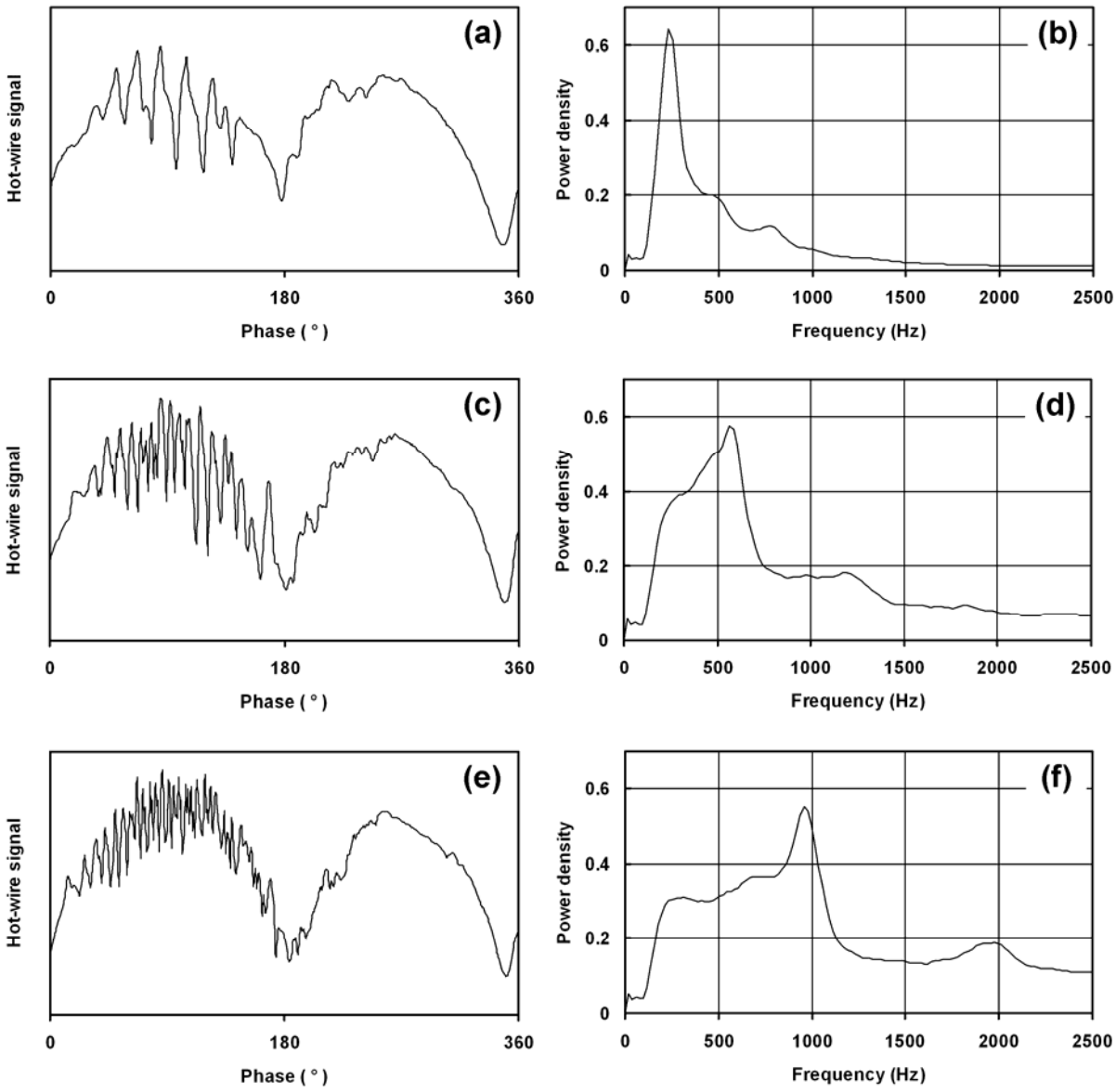

Figure 6 Hot-wire signal traces within an acoustic cycle and the corresponding frequency spectra of stack with d = 2mm, D = 4.8mm; a, b (Re = 550, Dr = 1.0%); c, d (Re = 1133, Dr = 2.0%); e, f (Re = 1774, Dr = 3.0%)

The Strouhal numbers obtained for all the flow cases related to stack B (i.e. 31 – 40 in Table 1), are calculated using Eq. (1). The relationship between the obtained Strouhal numbers versus Reynolds numbers is plotted using square symbols in Fig. 7. In addition, analogous results obtained using stacks A (flow cases 15 – 21 from Table 1) and C (flow cases 57 – 65 from Table 1) are also shown in Figure 7 as diamonds and triangles, respectively. It can be seen that in general terms Strouhal number increases as Reynolds number increases. While for stack B this dependence is practically monotonic, it is not for stacks A and C – some degree of "scatter" occurs around the underlying overall trend. However such "scattered" points can also be seen in the data obtained earlier by Mao et al. [18]. It is possible that such behaviour can arise from the variability in the underlying flow patterns, as well as shedding phenomena occurring in slightly different parts of the acoustic cycle – in other words the velocity amplitude not being fully representative of the shedding phenomena, for the purpose of obtaining Strouhal number values.

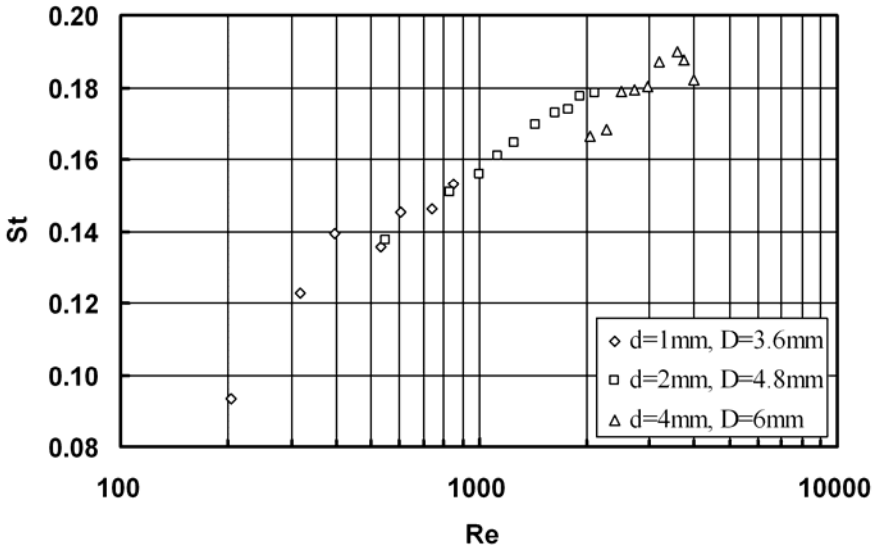

Figure 7 Variations of Strouhal number with Reynolds number for given configurations of stack

To expand the latter point further: it is believed that the relationship between St and Re is closely related to the vortex wake pattern transitions at the end of the stack. Earlier work [23] and [24] summarised the vortex wake pattern transitions (obtained, among others, for flow cases around stacks A, B and C). Here, as an example, three cases of flow patterns, obtained on stack C, are illustrated in Fig. 8 (for brevity only phases Φ_5 and Φ_9 are shown in each case). At the relatively small Reynolds number (flow case 61 in Table 1, Re = 2947, Fig. 8a and b), the vortex patterns over the ejection stage simply change from the attached symmetrical vortices (which are similar to those in Fig. 5a) to alternate shedding from both sides of the plate as shown in Fig. 8a. This flow pattern does not change until the flow reverses (vortex pattern in Fig. 8b does not change significantly, except that it propagates further downstream). At a higher Reynolds number (flow case 63, Re 3573, Figs. 8c and d), the alternate vortex shedding patterns dominate in the ejection stage. The Strouhal number increases as would be expected from a higher value of the velocity amplitude (cf. Fig. 7). However, at the highest Reynolds number studied for stack C (flow case 65, Re 3968, Figs. 8e and f), the vortex

Advance Manuscript

patterns of the alternate shedding (Fig. 8e) evolve into elongated vortex structures (Fig. 8f) in the deceleration stage, or in other words the shedding of discrete vortices stops earlier within the cycle compared to previous cases. However, despite the change in the flow physics, Eq. (1) is used indiscriminately to calculate St, which may lead to somewhat "scattered" (non-monotonic) behaviour of St vs. Re dependence. The problem of changing flow physics is illustrated in Fig. 9 by selecting the hot-wire signals for flow cases 63 and 65. It can be seen that both the timing of the fluctuations within the cycle and the length of time when the representative fluctuations take place are different in different flow situations. For example, the representative fluctuations for the flow case 63 in Fig. 9a (i.e. those ultimately defining St) appear mostly in the deceleration stage. The representative fluctuations for the flow case 65 in Fig. 9b only cover the end of acceleration and beginning of deceleration. The representative (or main) fluctuations are marked in Fig 9 by the label "fluctuation time". This is not to say that there are no fluctuations outside these marked periods, but that the ones outside may not be the ones that should really define the Strouhal number.

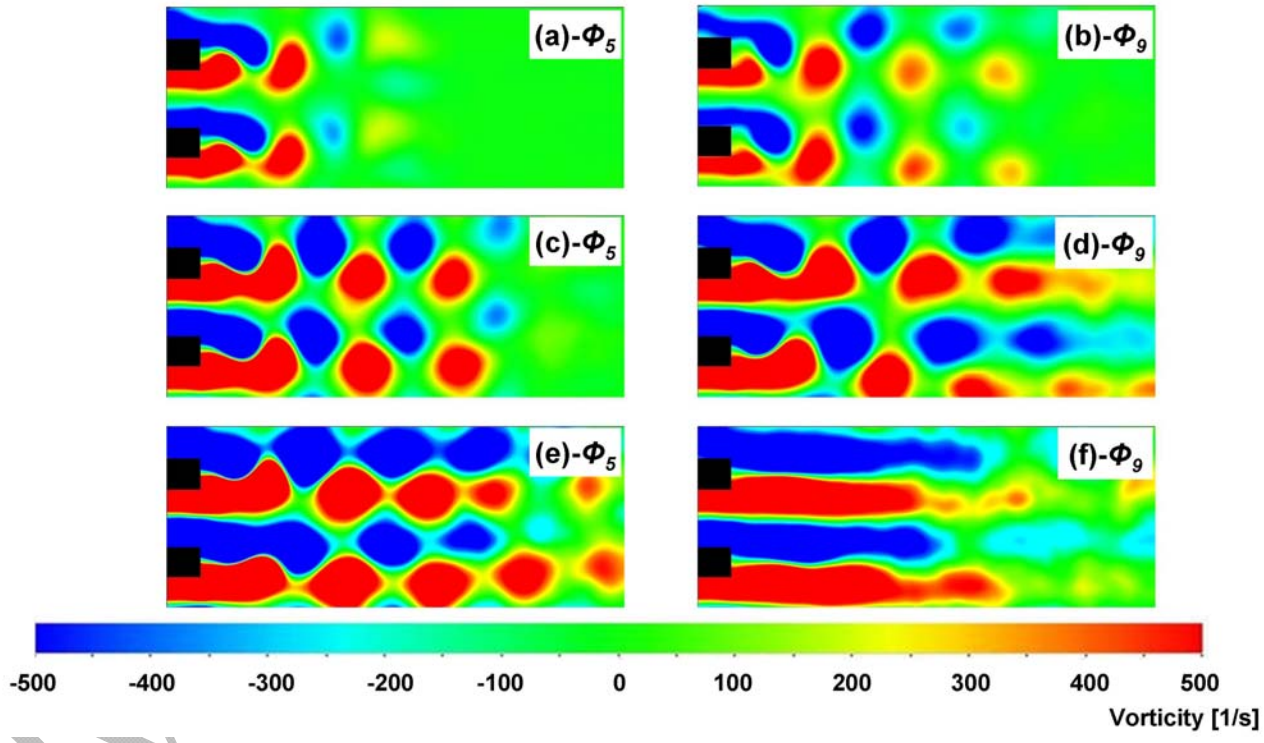

Figure 8 Vorticity fields for the flow at the end of the stack with d = 4mm, D=6mm; a, b (case 61); c, d (case 63); e, f (case 65)

It is possible that graphs such as those shown in Fig. 7 should ideally be corrected by choosing an "instantaneous" reference velocity, together with an "instantaneous" shedding frequency. While in principle using an instantaneous velocity as a reference is possible, the frequency is in practice obtained through appropriate FFT techniques that require blocks of data of finite length (duration). Furthermore, the frequency resolution depends on both the sampling rate and the length of the data blocks. These limitations make the idea of "tuning" the velocity and frequency to provide more

Advanced Manuscript

accurate estimates of St simply impractical. Furthermore, if only corrections to the velocity were sought, it would be far too complicated to "guess" the correct reference velocity having only the hot-wire signals at one's disposal and normally not knowing the flow physics a priori.

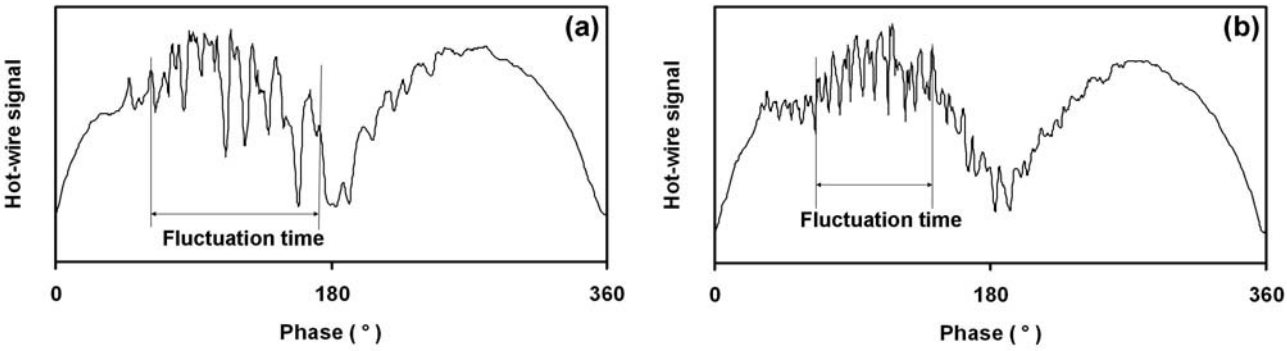

Figure 9 Hot-wire signals within an acoustic cycle for stack C: a – case 63; b – case 65

For the flow cases of stacks A and B, the variations of the Strouhal numbers with the Reynolds numbers could be also associated with the type of vortex patterns present (and the difficulties with selecting the "correct" reference velocities). For stack A, at the relatively small Reynolds numbers, the vortex patterns in the ejection stage evolve from attached symmetrical vortex structures to elongated vortex structures, then a "break-up" of elongated vortices into a vortex street. At relatively large Reynolds numbers, the break-up of elongated vortices further develops into alternate shedding from the top and bottom side of the plate. This change in vortex shedding modes might result in the "scatter" of Strouhal numbers shown in Fig. 7 for stack A. For the flow cases of stack B, the vortex patterns always develop from the attached symmetrical vortex structures to alternate shedding when the Reynolds number increases. This unambiguous vortex pattern behaviour may be responsible for a well-behaved (monotonic) dependence of St vs. Re.

An interesting point related to data presented in Figure 7 is the actual dependence of Strouhal on Reynolds number. For example for a selected case of d = 2 mm (stack B), one can clearly see that St increases from around 0.14 to 0.18 with Re changing from around 500 to 2,000. This is purely an effect of increasing the velocity amplitude in a given geometrical configuration (nothing else changes in the system). Interestingly, according to the definition by Merkli and Thomann [25] the local Reynolds number (which they denote A) would vary between 213 and 821 and so during the experiment the transition condition of A = 400 would have been reached. However, this does not seem to affect the continuity of the St vs. Re curve, which in turn may indicate that turbulent transition is not a major factor in defining dependence.

Advanced Manuscript

Unfortunately, the above does not reveal the actual mechanisms behind the change in St. One could hypothesise that as the velocity amplitude changes, the length of the "closed wake" part of the flow field (i.e. between the plate end and the confluence point, cf. [26]) changes, which results in turn in different sizes of the eddies being shed. The net effect could be the observed variation in St vs. Re dependence.

It is also interesting to make qualitative comparisons with vortex shedding in steady flows. In the flow past a circular cylinder, Roshko [4] observed a relatively sharp increase in St from ~0.12 to ~0.18 as Re (based on the cylinder diameter) varied between 40 and 150. Clearly, any comparisons between oscillatory flows past plate stacks and steady flows past a circular cylinder must be done extremely cautiously: Roshko's data is for laminar shedding, and the respective Reynolds numbers do not necessarily mean the same, but it is encouraging that on the phenomenological level St vs. Re dependence is not dissimilar. However, even for a "simple" case of vortex shedding from a circular cylinder in a steady laminar situation, there is no simple explanation as to why St changes with Re in the way it does. Therefore it may be equally challenging to explain the behaviour of St vs. Re in an oscillatory flow.

3.3 The relationship between St and d/(d+D).

In the classical studies of vortex shedding from bluff bodies, one of the investigated characteristics is the influence of the blockage ratio on Strouhal number, i.e. change of vortex shedding frequency in response to changing the geometrical factor d/H, where d and H are characteristic dimensions of the bluff body and the transverse dimension of the test section where the investigations are carried out. Examples of such measurements are given by West and Apelt [6] and Al-Asmi and Castro [8], who investigated the effects of wind tunnel blockage ratios on Strouhal numbers arising from vortex shedding from both circular and non-circular cylinders. In studies of this kind the data is typically plotted as the variation of St vs. Re at a constant blockage ratio, or St vs. blockage ratio with Re kept constant.

In the current flow arrangement the situation is somewhat different for two reasons: the flow is oscillatory rather than steady and the vortex shedding is investigated on an array of bluff bodies (series of plates) rather than a single obstacle. The first issue has already been addressed in previous sections. The second problem, of having multiple bodies, needs to be addressed by defining the blockage ratio as the cross sectional area of he plates in the stack over the cross sectional area of the acoustic resonator, which can be approximated by the ratio $d/(d+D)$. In this context the blockage effects can be understood as a change in vortex shedding behaviour on a selected plate due to the presence (proximity) of neighbouring plates in the stack.

Advanced Manuscript

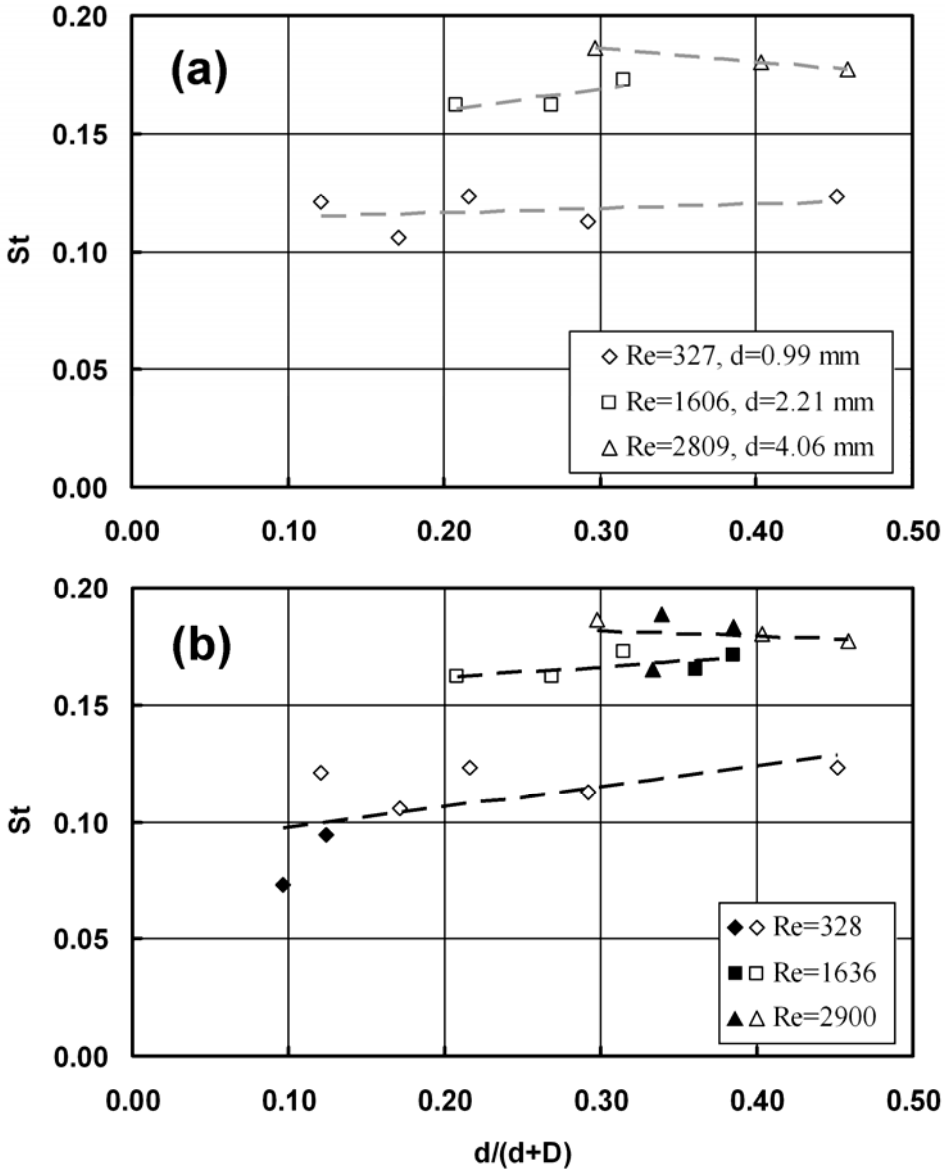

Figure 10 Dependence of St on blockage ratio, *d/(d+D)*, at a constant Re: a – comparisons based on cases with the same plate thickness taken for Re calculations; b – comparisons based on cases of similar Re, without maintaining constant plate thickness.

The data for analysis has been selected to study the dependence of Strouhal number on blockage ratio at an almost constant Reynolds number (an exact value of Reynolds number would be difficult to maintain as generally u_{aM} would not be known prior to taking PIV data – the experiments were only controlled using Dr). However an additional precaution was taken to keep the plate thickness constant (not just the Reynolds number, i.e. in effect the product of d and velocity amplitude), because it is known [23, 24] that the oscillatory flow studied here exhibits a range of different flow patterns and flow pattern transitions when the stack geometry varies. Keeping the plate thickness constant was thought to ensure that in the initial studies the actual effects of blockage can be separated from the flow pattern

transition effects. Three levels of Re have been selected using Table 1 as follows: low range, with average Re=327 comprising of cases 9 (Re=328), 11 (Re=281), 16 (Re=318), 22 (Re=323) and 25 (Re =386); medium range, with average Re=1606 comprising of cases 37 (Re=1638), 43 (Re=1666) and 46 (Re=1513); and high range, with average Re=2809 comprising of cases 56 (Re=2514), 61 (Re=2947) and 72 (Re=2966).

Figure 10a shows the dependence of St vs. blockage ratio for three cases of Re number, for cases where plate thickness was kept constant. As can be seen, the general trend is that as Re level increases, so does St (cf. the three different Strouhal number levels for diamond, square and triangle symbols). However, more importantly for a given Re (plate thickness) the change of St with blockage ratio is very weak. It seems there is a slight increase in St with blockage ratio for Re=327 and Re=1606, while there is a slight decrease for Re=2809. Grey dashed lines illustrate the least square fit lines based on the experimental results.

It is also possible to introduce into the plot the points corresponding to similar levels of Re, but based on the cases where the plate thickness is different (Figure 10b). Black diamonds represent two additional cases (7 and 8) where the plate thickness was 0.51 mm; black squares represent two additional cases (48 and 67) where the plate thickness was 3 and 4.06 mm, respectively; and finally black triangles represent three additional cases (50, 51 and 74) where the plate thickness was 3 mm for the first two cases and 5.12 mm for the latter case. As can be seen the trend lines (black dashed lines) change somewhat, probably the most pronounced change being visible for the lowest level of Re. This is due to the new points being far off the original trend line, which may represent a difference in the vortex shedding flow physics, although it is difficult to speculate on the exact reasons on the basis of available data.

It is interesting to note that in the context of oscillatory flows past parallel plate stacks, the already mentioned work by Worlikar et al. [21] studied the effect of blockage ratio on the flows in the stack vicinity, but unfortunately the study was concerned with very small drive ratios and so strictly there were no “vortex streets” observed and comparisons with current work would be rather difficult. Besnoin and Knio [22] investigated a rather more complex case where both the fluid flow and thermal effects were considered in a more complicated geometry which included both the stack and heat exchangers. The dependence of the thermal performance on the plate thickness and plate spacing parameters (and in particular blockage ratio) was studied, but in doing so the fluid dynamical phenomena were not discussed in any detail. Therefore, it is difficult to make meaningful comparisons between current work and results presented in [22].

Advanced Manuscript

3.4 The complete map of the relationship between Re and St

In his studies of vortex shedding from circular cylinders in steady flows, Roshko [4] obtained a widely accepted correlation between the Strouhal number and Reynolds number, for two different flow regimes as discussed in the introduction section, in the following form:

$$St = 0.212(1 - 21.2/Re) \qquad \text{for } 50 < Re < 150 \qquad (3)$$

$$St = 0.212(1 - 12.7/Re) \qquad \text{for } 300 < Re < 2{,}000 \qquad (4)$$

In the current study, there exists a number of different flow regimes, as discussed in [23] and [24], which may be controlled not only by the peak Reynolds number itself, but also other similarity parameters such as Keulegan-Carpenter number or porosity, as discussed in [18] and [20]. Nevertheless, it may be useful to present all the 76 cases studied in terms of the dependence of St vs. Re in one graph such as Figure 11 (the additional legend allows identifying the six different plate thickness values). 7% error bars have been added based on the error analysis that estimates the uncertainty of peak frequency identification at 5% and the velocity amplitude identification at point M at 2%.

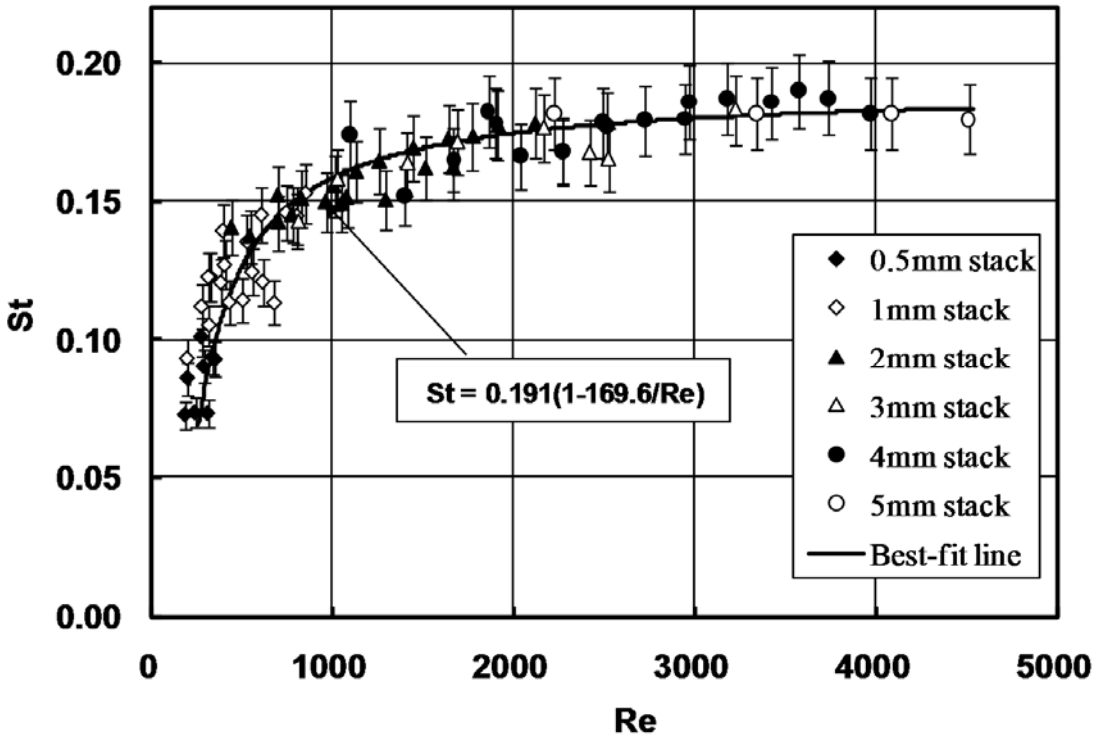

Figure 11 Strouhal vs. Reynolds number for the oscillatory flow cases covered in the current study

It is clear that the Strouhal number increases gradually with the increase of Reynolds number between 200 and 5,000, but seems to saturate at the level close to 0.2, which is congruent with Strouhal number behaviour in steady flows. However, as discussed in section 3.2, for each plate thickness, the Strouhal number does not increase completely

Accepted manuscript

monotonically, giving a certain "scatter" around the imagined overall trend, which may be associated with relatively more complex flow structures and their transitions than is seen in steady flows (or the difficulties with finding the correct reference velocities and frequencies). By analogy to equations (3) and (4), it is also possible to fit the experimental data into a least square fit line of the same mathematical form as used by Roshko [4]. The resulting equation:

$$St = 0.191(1 - 169.6/Re) \qquad \text{for } 200 < Re < 5{,}000 \qquad (5)$$

is represented in Figure 11 by a solid black line.

4. Conclusion

The current study addresses the problem of vortex shedding from the stack of parallel plates in the oscillatory flow condition imposed by an acoustic standing wave. It should be noted that the vortex shedding processes in the oscillatory flow are much more complicated than those in steady flows and as a result there is a much wider selection of characteristic vortex patterns and their evolution paths. However the main motivation of this work is to investigate whether the vortex shedding processes can be characterised in terms of the Strouhal number using an analogous methodology and similar concepts to those used for steady flows. The experimental approach used included measuring the velocity fluctuations arising from vortex shedding processes, using hot-wire anemometry techniques, while an additional insight into the flow physics was obtained by using PIV.

In this study, the Strouhal number was defined using the predominant vortex shedding frequency obtained through FFT analysis of the hot-wire signal and the local acoustic velocity amplitude, as these are straightforward quantities that can be obtained experimentally. By changing the intensity of acoustic excitation and the stack configuration (plate thickness and plate spacing), it was possible to investigate the relation between the Strouhal and Reynolds numbers using 76 different flow cases. In this sense, this work is the first systematic investigation of this kind, conducted for a wide range of geometrical and excitation parameters.

Following the conventions used in steady flows, the complete map of the relationship between the Strouhal number and Reynolds number for all cases studied has been captured, together with a mathematical expression obtained through least square fit methods for $200 < Re < 5{,}000$, as illustrated in Figure 11. The general trend is the increase of Strouhal number with Reynolds up to a certain "saturation" level around 0.2, which is somewhat similar with the trend found in steady flows. It seems plausible to that the flow physics controlling the vortex shedding frequency in the "ejection"

Advanced Manuscript

stage of the oscillation cycle is similar to that for steady flows. Referring back to the key question highlighted at the end of section 1, it seems there is a relatively smooth change of St vs. Re over the whole Re range, not a step-change (a threshold behaviour) as hypothesised in previous work based on a very fragmentary set of experiments [18].

The second issue investigated in the current work is the dependence of St on the stack blockage ratio at constant Reynolds number. It seems that such dependence is relatively weak however it is also shown that St can either increase or decrease with blockage ratio depending on particular stack configurations. The reason for this behaviour is not well understood and would require further studies of the underlying flow physics. A further complication arises, because Re does not seem to describe the flow unambiguously which can be clearly seen by comparing Figs. 10a and b for the lowest range of studied Reynolds numbers: a change in plate thickness produces a different relation between St and blockage ratio.

Finally, it should be noted that defining the Strouhal number as described in this paper is somewhat arbitrary. It could be argued that as the instantaneous acoustic velocity changes, one would have to vary the reference velocity. On the other hand, as the velocity varies, so does the instantaneous shedding frequency, and the latter should be taken into the Strouhal number calculations. However, taking or finding such instantaneous values would be rather impractical as discussed in section 3. Thus the current approach may in some sense produce temporally averaged Strouhal numbers, resulting in somewhat scattered data points in Figure 11. It may also be the reason for a somewhat ambiguous dependence of St on blockage ratio. Further work to unravel these effects is required.

Acknowledgements:

The authors would like to thank the European Commission for supporting this work under FP7 grant number 226415 (THATEA); the Universities UK for the ORS scholarship of the first author and the University of Manchester for matching funding towards ORS. Professor Brian Launder is acknowledged for useful discussions regarding St vs. Re dependence.

References:

[1] **Strouhal, V.** Ueber eine besondere Art der Tonerregung, *Annalen der Physik und Chemie*, 1878, **5** (10) (1878), 216–251.

[2] **Rayleigh, L.** *The Theory of Sound*, 1945 (Dover Publications, New York).

Advanced Manuscript

[3] **Kovasznay, L.S.G.** Hot-Wire Investigation of the Wake behind Cylinders at Low Reynolds Numbers. *Proceedings of the Royal Society of London. Series A, Mathematical and Physical Sciences (1934-1990)*, 1949, **198**(1053), 174-190.

[4] **Roshko, A.** On the Development of Turbulent Wakes from Vortex Streets. National Advisory Committee for Aeronautics. *NACA Tech Report 1191*, 1954.

[5] **Williamson, C.H.K.** The existence of two stages in the transition to three dimensionality of a cylinder wake. *Physics of Fluids*, 1988, **31**, 3165-3168.

[6] **West, G.S.** and **Apelt, C.J.** The effects of tunnel blockage and aspect ratio on the mean flow past a circular cylinder with Reynolds numbers between 10^4 and 10^5. *Journal of Fluid Mechanics*, 1982, **114**, 361-377.

[7] **Okajima, A.** Strouhal numbers of rectangular cylinders. *Journal of Fluid Mechanics*, 1982, **123**, 379-398.

[8] **Al-Asmi, K.** and **Castro, I.P**. Vortex shedding in oscillatory flow: geometrical effects. *Flow Measurement and Instrumentation*, 1992, **3**(3), 187-202.

[9] **Ferreira, R.L.** and **Vieira E. D. R.** Flow around modified circular cylinders. *Thermal Engineering*, 2004, **5**, 62-67.

[10] **Williamson, C.H.K.** and **Roshko, A.** Vortex formation in the wake of an oscillating cylinder. *Journal of fluids and structures*, 1988, **2**(4), 355-381.

[11] **Okajima, A.**, **Matsumoto, T.** and **Kimura, S**. Force measurements and flow visualization of bluff bodies in oscillatory flow. *Journal of Wind Engineering & Industrial Aerodynamics*, 1997, **69**, 213-228.

[12] **Chung, Y.J.** and **Kang, S.H.** A Study on the Vortex Shedding and Lock-on behind a Square Cylinder in an Oscillatory Incoming Flow. *JSME International Journal Series B*, 2003, **46**(2), 250-261.

[13] **Barbi, C.**, **Favier, D. P.**, **Maresca, C. A.**, and **Telionis, D. P.** Vortex shedding and lock-on of a circular cylinder in oscillatory flow. *Journal of Fluid Mechanics*, 1986, **170**, 527-544.

[14] **Swift, G.W.** Thermoacoustic engines. *The Journal of the Acoustical Society of America*, 1988, **84**, 1145-1180.

[15] **Swift, G.W.** *Thermoacoustics: A Unifying Perspective for Some Engines and Refrigerators*, 2002 (Acoustical Society of America, New York).

[16] **Blanc-Benon, P.**, **Besnoin, E.**, and **Knio, O.** Experimental and computational visualization of the flow field in a thermoacoustic stack. *Comptes rendus-Mecanique*, 2003, **331**(1), 17-24.

[17] **Berson, A.** and **Blanc-Benon, P.** Nonperiodicity of the flow within the gap of a thermoacoustic couple at high amplitudes. *The Journal of the Acoustical Society of America*, 2007, **122**(4): EL122-EL127.

[18] **Mao, X.**, **Yu, Z.**, **Jaworski, A. J.**, and **Marx, D.** PIV studies of coherent structures generated at the end of a stack of parallel plates in a standing wave acoustic field. *Experiments in Fluids*, 2008, **45**, 833-846.

Advanced Manuscript

[19] **Aben, P.C.H.**, **Bloemen, P.R.**, and **Zeegers, J.C.H.** 2-D PIV measurements of oscillatory flow around parallel plates. *Experiments in Fluids*, 2009, **46**(4), 631-641.

[20] **Shi, L., Yu, Z., Jaworski, A. J.** Vortex shedding flow patterns and their transitions in oscillatory flows past parallel-plate thermoacoustic stacks. *Experimental Thermal and Fluid Science*, 2010, **34**(7), 954-965.

[21] **Worlikar, A.S.**, **Knio, O.M.**, and **Klein, R.** Numerical simulation of a thermoacoustic refrigerator. I. unsteady adiabatic flow around the stack. *Journal of Computational Physics*, 1996, **127**(2), 424-451.

[22] **Besnoin, E.** and **Knio, O.M.** Numerical study of thermoacoustic heat exchangers. *Acta Acustica united with Acustica*, 2004, **90**(3), 432-444.

[23] **Mao, X.**, **Shi, L.**, **Yu, Z.**, and **Jaworski, A. J.**, Investigations of flow morphology around thermoacoustic parallel-plate stacks and heat exchangers. SEM Annual Conference, Albuquerque, New Mexico USA, 1-4 June, 2009.

[24] **Shi, L., Yu, Z., Jaworski, A. J.** Vortex formation at the end of parallel-plate stack in the standing-wave thermoacoustic device. The Sixteenth International Congress on Sound and Vibration, Krakow, 5-9 July, 2009.

[25] **Merkli, P.**, and **Thomann, H.** Transition to turbulence in oscillating pipe flow. *Journal of Fluid Mechanics*, 1975, **68**, 567-576.

[26] **Mao, X.,** and **Jaworski, A. J**. Oscillatory flow at the end of parallel plate stacks – phenomenological and similarity analysis. *Fluid Dynamics Research*, 2010, **42**, 055504.

Advanced Manuscript